

## Reflectionless Tunneling at the Interface between Nanoparticles and Superconductors

J. L. Dunford and A.-A. Dhirani\*

*Department of Chemistry, University of Toronto, Ontario, Canada, M5S 3H6*

(Received 25 September 2007; published 8 April 2008)

Interfaces between disordered normal (DN) materials and superconductors ( $S$ ) are known to generate conductance peaks at zero-bias voltage ( $V$ ) and magnetic field ( $B$ ). Using molecularly linked Au nanoparticle films as the DN component, we find that superimposed on conductance peaks are oscillations that depend simultaneously on both  $V$  and  $B$ . Such correlated conductance oscillations are predicted by a “reflectionless tunneling” phenomenon but have not been observed in other DN- $S$  systems. Length scales extracted from periods of conductance oscillation correlate well with film nanostructure.

DOI: [10.1103/PhysRevLett.100.147202](https://doi.org/10.1103/PhysRevLett.100.147202)

PACS numbers: 75.75.+a, 73.23.-b, 73.63.-b, 74.45.+c

Historically, interfaces between superconductors ( $S$ ) and normal ( $N$ ) materials have proven to be fertile ground for revealing new superconducting phenomena and for gaining new insights into superconductivity. In the 1990s, Kastalsky *et al.* and Magnée *et al.* observed a new mesoscopic phenomenon in such systems: Zero-bias conductance peaks (ZBCPs) can be generated at  $\text{In}_{0.53}\text{Ga}_{0.47}\text{As}$ -Nb and doped Si-Nb interfaces, respectively [1,2]. Their results suggested that phase coherent processes at the interface are important at low bias. This phenomena was then interpreted by van Wees *et al.* [3], Beenakker *et al.* [4], and Marmorkos *et al.* [5], who developed various treatments of a “relectionless tunneling” (RT) model. In this model, a ZBCP is generated by an Andreev reflection (AR) process enhanced by elastic scattering in the normal region. That is, at disordered normal (DN)- $S$  interfaces, electrons have multiple opportunities to attempt AR. If they fail an initial attempt, they are specularly reflected from  $S$ , coherently scattered off dopants and/or defects in DN, and redirected towards the interface to reattempt AR. In doped semiconductors, elastic scattering lengths ( $L_e$ s) tend to be large (100 s of nm), and ZBCP widths tend to be correspondingly narrow. Frydman and Dynes used granular Ag films and Pb superconducting contacts to explore this RT phenomenon [6]. As film thickness increased, conductance vs voltage measurements exhibited ZBCPs consistent with RT for a narrow range of thicknesses. This behavior supports a RT model since it correlates conductance features with film disorder. Note that a feature of granular metal films is that their short  $L_e$ s yield correspondingly broad, robust ZBCPs.

A number of processes besides RT are known to generate ZBCPs. These include electron-electron scattering [7–10], AR [11–14], and spin-polarization enhanced AR [15,16]. van Wees *et al.*, however, predicted a hallmark of RT: An electron successfully undergoing AR generates a hole that travels the electron’s time-reversed pathway and interferes with the electron [3]. The treatment considered electrons and holes propagating freely as plane waves that scatter classically in DN at defects larger than the Fermi wavelength,  $\lambda_F$ . In the presence of an applied voltage ( $V$ ) and

magnetic field ( $B$ ), this semiclassical treatment shows that electron-hole wave functions are phase shifted by  $\Delta\phi$ :

$$\Delta\phi = \frac{2e}{\hbar} \left( \frac{VL^*}{v_F} + BA \right), \quad (1)$$

where  $\hbar$  is the reduced Planck constant,  $e$  is the elementary charge constant,  $v_F$  is the Fermi velocity in DN,  $L^*$  is the path length between attempts at AR processes, and  $A$  is the area enclosed between this path and the DN- $S$  interface [3,17]. As a result, conductance is predicted to exhibit quantum electro-magneto-conductance oscillations (QEMCO), i.e., correlated conductance oscillations as a function of both  $V$  and  $B$ . In previously studied DN- $S$  (e.g., doped semiconductor- $S$  and thermally deposited granular metal film- $S$ ) systems, averaging over  $L^*$  gave rise to rapid dephasing as fields increased, and conductance vs. field yielded just a peak at zero field [1,2,6,12,13,18,19]. In order to observe QEMCO due to RT, the scattering site (defect) density should be sufficiently large to induce multiple AR attempts, but the distribution of  $L^*$  should be sufficiently narrow to restrict dephasing.

We show here that a novel “artificial material” comprising prefabricated 5 nm Au nanoparticles that are subsequently cross-linked with 1,4-butanedithiol molecules ( $[\text{HS}-(\text{CH}_2)_4\text{-SH}]$ ) enables direct observation of QEMCO. Independent estimates of path lengths obtained through both  $V$  and  $B$  measurements are consistent with known nanostructure of the films. The effect is observed routinely, is robust, and persists to large  $V$  and  $B$ , remarkably even beyond the bulk critical field values ( $H_c$ s) of the  $S$  components. We propose that this might be due to the nanostructured nature of the DN- $S$  interface. Our present study exploring superconducting phenomena, combined with previous studies demonstrating both Mott- and percolation-driven metal-insulator transitions [20–24], quantum interference effects (i.e., “weak localization”) [25], and a rich array of nanoparticle properties demonstrate that such novel self-assembled molecularly-linked nanoparticle films (NPFs) are a useful test bed for exploring charge transport in general. A wide choice of material

components, including semiconducting, superconducting, or ferromagnetic nanoparticles, is readily available.

Nanoparticles can be purchased or easily fabricated via well-established methods. Here, Au nanoparticles ( $4.8 \text{ nm} \pm 1.2 \text{ nm}$  in diameter) were prepared in toluene as in Ref. [22]. Details of butanedithiol-linked Au NPF preparation can be found in Refs. [25–27]. We used two superconductors for contacts: In (99.999% pure) was purchased from ESPI; InPbSn (45:20:35 by weight) was prepared by mixing In with PbSn solder (37:63 by weight) at  $\sim 600 \text{ K}$ . In has  $T_{\text{melt}} \approx 430 \text{ K}$ ,  $T_c = 3.37 \text{ K}$ , and  $H_c = 19 \text{ mT}$ , while InPbSn has  $T_{\text{melt}} \approx 420 \text{ K}$ ,  $T_c = 6.68 \text{ K}$ , and  $H_{c1} = 520 \text{ mT}$ , as determined by bulk ac magnetic susceptibility. Both four- and two-probe electrode geometries were used. For the former,  $S$  was directly contacted to NPFs. For the latter, round Au pads (1.5 mm in diameter, 150 nm thick) were thermally deposited approximately 5 mm apart on each NPF. For these samples, In or InPbSn was contacted to both the NPF and the Au pads, which served as soldering anchors. Four-probe samples without Au anchors were also prepared and exhibited similar results to those with anchors [27]. However, unanchored contacts often became unattached during cooling. For control samples,  $S$  contacted elongated Au pads that partially overlapped the NPFs such that direct NPF- $S$  contact was avoided. For all cases, Cu magnet wires (100  $\mu\text{m}$  thick) contacted the superconductors.

$T$  and  $B$  were controlled by a Quantum Design physical property measurement system (PPMS)  $^4\text{He}$  cryostat equipped with a 14 T Oxford Instruments magnet. Differential conductance ( $g$ ) was measured using standard lock-in techniques at low frequencies where  $g$  varied slowly with frequency (typically 100 to 1000 Hz). We confirmed reproducibility by testing 15 two-probe samples prepared with 5 to 10 alternating butanedithiol-nanoparticle immersion cycles. NPFs were stable over many cycles of  $V$ ,  $B$ , and  $T$ .

Figure 1(a) shows a plot of two-probe  $g$  vs  $V$  ( $B = 0$ ,  $T = 2.0 \text{ K}$ ) using a five-exposure NPF with In contacts acting as the  $S$  components (Sample 1). The plot exhibits a ZBCP with a height of 3.9% and a width of  $\pm 380 \text{ mV}$ . Two thirds of similar devices exhibited comparable ZBCPs with heights and widths ranging from 0.2% to 10% and 0.20 to 1.0 V, respectively. The range of observed behaviors is an indication of the importance of disorder in these systems, as discussed further below. The plot in Fig. 1(a) also exhibits broad shoulders at  $\sim \pm 1 \text{ V}$ . The same peak exhibits a  $B$  dependence as well. Figure 1(b) shows a plot of magnetoconductance,  $g$  vs  $B$ , at various  $V$  for the same sample. At  $V = 0 \text{ V}$ , the data exhibit a zero-(magnetic) field conductance peak (ZFCP). As  $V$  increases, the shape of the magnetoconductance changes until at  $V = 0.4 \text{ V}$ , it has evolved into a valley, and then at 0.8–1.0 V back to a (much smaller) peak again. Note that these  $V$ 's are correlated with features in Fig. 1(a): When  $g$  is a maximum (minimum) with respect to  $V$ , magnetoconductance exhibits a peak (valley) at  $B = 0$ . This correlation suggests that

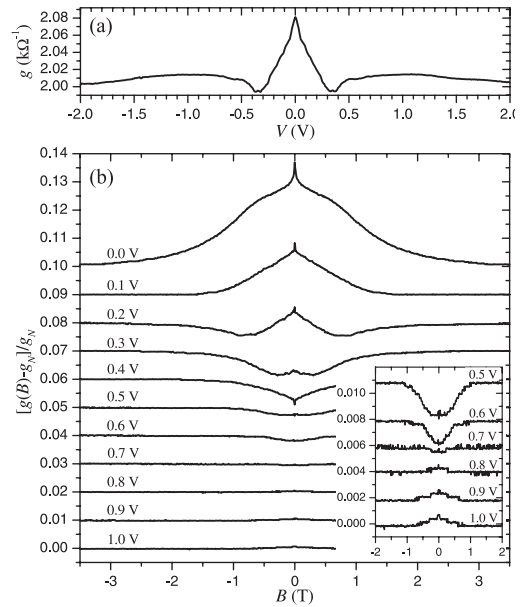


FIG. 1. (a) A ZBCP in  $g$  vs  $V$  (at  $B = 0$ ), and (b) ZFCPs in  $g$  vs  $B$  (for several  $V$ ) observed at 2.0 K for sample 1. Data in (b) have been normalized to high  $|B|$  values and offset by 0.01 for each  $V$  (main panel), and by 0.002 for 0.6 V to 1.0 V and 0.003 for 0.5 V (inset), for clarity.  $g$  was approximately constant for  $4 \text{ T} \leq |B| \leq 14 \text{ T}$ .

the broad shoulders in Fig. 1(a) are actually “peaks” above the background conductance obtained at high  $|B|$  or  $|V|$ .

Since they vanish at  $T_c$  [27], the observed ZBCP and ZFCP fundamentally originate from superconductivity of the contacts [13,27]. We confirmed this using several samples and superconducting contacts with different  $T_c$  (In and InPbSn). The effects arise, in particular, at the NPF- $S$  interface. Film conductance, isolated from interface conductance through four-probe measurements, did not exhibit conductance peaks [27]. Also, control samples with  $S$  contacting Au pads but not directly contacting the NPF itself did not exhibit such features. We also studied seven thermally deposited Au films ranging in thickness from 16 to 60 nm. Only two of the thinnest films (16 and 20 nm) exhibited conductance peaks with fine features [27]. The others exhibited peaks consistent with Blonder-Tinkham-Klapwijk theory [28], or sometimes no peaks at all. This highlights the importance of the nanograins at the interface. In thicker thermally deposited films, scattering from nanoscale defects (grain boundaries) becomes insignificant. In contrast, in NPFs, scattering remains important even in thick films, and such conductance features are common.

The oscillatory behavior of ZBCP and ZFCP shown in Fig. 1 reveals that the features found in the present study arise fundamentally from interference, and their dependencies on both  $V$  and  $B$  are consistent with QEMCO [see Eq. (1)]. Observation of QEMCO in macroscopic NPF- $S$  systems is remarkable since it implies reduced averaging over length scales. This can be attributed to (i) use of

nanoparticles with sufficiently narrow size (and therefore  $L_e$ ) distributions; (ii) reduced current pathways, as films self-assembled “layer-by-layer” are highly porous (shown in previously published SEM [20] and STM [27] images); and (iii) a tendency of organic cross-linkers to reduce wettability of  $S$  on the NPF, further reducing the number of pathways traversed by charges near the NPF- $S$  interface. In conventional disordered materials such as thermally deposited films and doped semiconductors, averaging over  $L^*$  results in dephasing at large fields. Thus, only a peak around zero field survives, and conductance oscillations are rarely observed [3,17]. Here, all 15 samples studied exhibited evidence of QEMCO, with different degrees of contrast corresponding to different distributions of  $L^*$ . Figures 2 and 3 illustrate the range of behaviors observed. Figures 2(a) and 2(b) show  $g$  vs  $V$  data at  $B = 0$  using 10- and 6-exposure samples, respectively. Both used InPbSn contacts. Data in Fig. 2(a) exhibit a ZBCP and several strong oscillations with multiple distinct periods. Fourier analysis (inset) yields periods of 160 mV, 100 mV, 83 mV, 71 mV, 45 mV, and 42 mV. In Fig. 2(b), we again observe a strong ZBCP along with finer features at higher  $|V|$ , implying a broader distribution of  $L^*$ .

Figures 3(a) and 3(b) show magnetoconductance at various  $V$ s using the same samples, respectively, as in Figs. 2(a) and 2(b). For both samples, there is a ZFCP that washes away with increasing  $V$ . Again, features are strongly correlated with  $V$ -dependent measurements. For example, in Fig. 3(a), sharp peaks occur at  $B = 0$  in  $g$  vs  $B$  data when  $V = 0.00, 0.20, 0.30,$  and  $0.40$  V, and at these voltages,  $g$  vs  $V$  data exhibit maxima [Fig. 2(a)]. Distinct multiple periods in  $V$  indicate the presence of a multimodal distribution of path lengths near the DN- $S$  interface in this sample. Figure 3(b) exhibits fine “oscillations” when

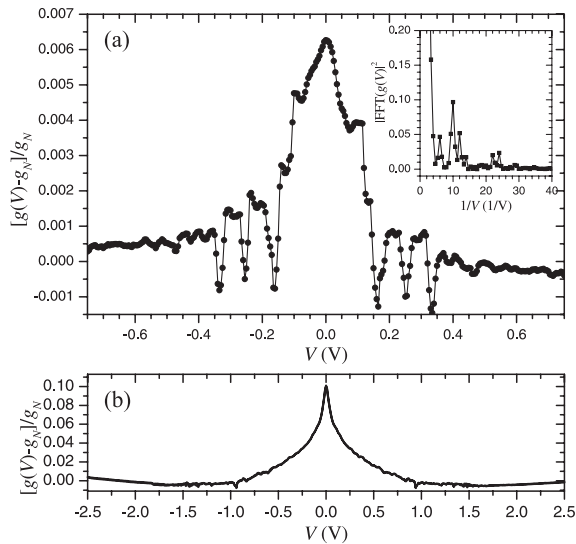


FIG. 2.  $g$  vs  $V$  ( $B = 0$ ) normalized to high  $|V|$  values for two Au nanoparticle film-InPbSn superconductor samples: (a) Sample 2 ( $T = 2.2$  K), and (b) Sample 3 ( $T = 2.75$  K). (Inset) FFT power spectrum of data in (a).

$0.70 \text{ V} \leq V \leq 1.45 \text{ V}$ , the same voltage range over which  $g$  vs  $V$  exhibits fine features [Fig. 2(b)]. To emphasize the oscillations and their anticorrelation as a function of  $V$  and  $B$  anticipated for QEMCO, Fig. 4 shows a color plot of  $\log|\partial^2 g/\partial B^2|$  vs  $V$  and  $B$  data for the sample used to obtain data in Figs. 2(b) and 3(b). Note that oscillations in  $g$ , indicated by points of inflection, move to lower  $|B|$  with increasing  $|V|$ . This indicates that a phase shift can be generated with contributions from either  $V$  or  $B$ , as in Eq. (1).

Periods of oscillation in  $g$  vs  $V$  and  $B$  can be used to estimate  $L^*$  independently through Eq. (1). Depending on the sample, periods in  $V$  range from  $\sim 50$  to  $\sim 500$  mV. Through four-probe measurements, we found that contact resistance was smaller than film resistance by a factor of order unity. Using Eq. (1) and taking  $v_F = 1.4 \times 10^6$  m/s with  $\Delta\phi = 2\pi$ ,  $B = 0$  and typical  $V_{\text{DN-S}} \approx 2V/7$  where  $V_{\text{DN-S}}$  is the voltage difference across the NPF- $S$  interface,  $L^*$  is estimated to range from 20 to 200 nm. Magnetoconductance data exhibit periods ranging from  $\sim 0.05$  T to  $\sim 1$  T. Using Eq. (1) with  $\Delta\phi = 2\pi$  and  $A = L^{*2}/2\pi$  yields  $L^*$  in the range from 18 to 180 nm [27]. In a strong diffusive limit, the upper bound of  $L^*$  can be estimated theoretically by

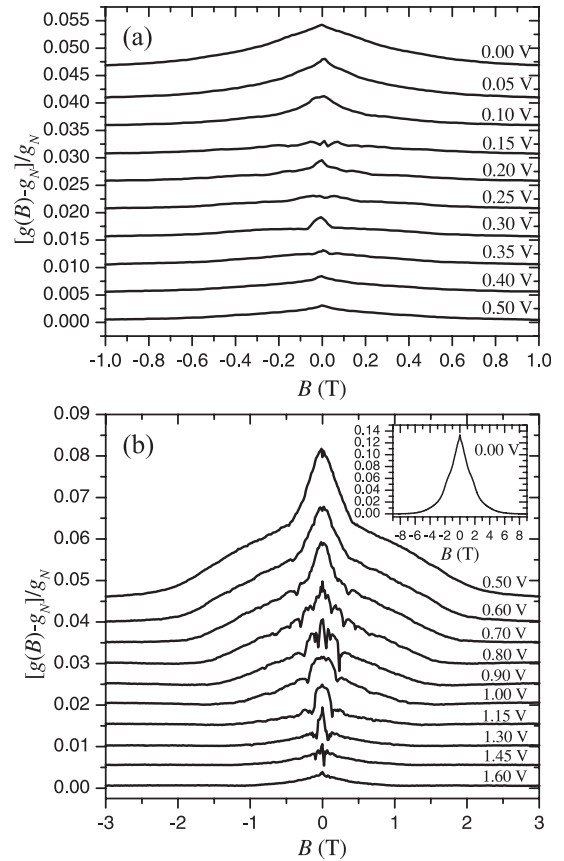


FIG. 3.  $g$  vs  $B$  (at several  $V$ ) normalized to high  $|B|$  values and offset by 0.005 for (a) sample 2 and (b) sample 3, each measured at the same temperatures as in Fig. 2. Only the ZFCP regions are shown.

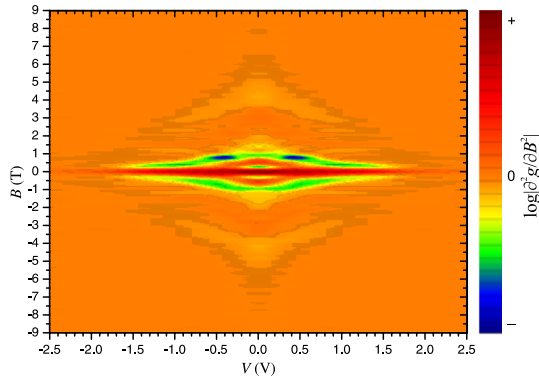


FIG. 4 (color online). Relief map of  $\log|\partial^2 g/\partial B^2|$  vs  $V$  and  $B$  at 2.75 K for Sample 3 showing correlated evolution of oscillatory features as a function of  $B$  and  $V$ . Red and blue regions represent large positive and negative values, respectively; orange represents 0.

$$L^* = \sqrt{\frac{\hbar v_F L_e}{3kT}}. \quad (2)$$

Taking  $L_e$  to be the average nanoparticle diameter yields  $L^* \sim 100$  nm at 2.0 K. These various independent estimates of  $L^*$  are consistent with each other and highlight a feature of NPFs:  $L^*$  values are sufficiently small and narrowly distributed that QEMCO are easily observed at relatively large  $V$  and  $B$ .

Remarkably, ZFCs persist to magnetic fields one to two orders of magnitude greater than  $H_c$  of InPbSn and In, respectively, where bulk type I superconductors become normal due to flux penetration. We also measured ZFCP widths of thermally deposited films of various thicknesses, and found that they too exceeded bulk  $H_c$  values but were systematically lower than those for NPF- $S$  systems [27]. Most thermally deposited films exhibited ZFCP widths  $< 0.5$  T, and only for the thinnest films ( $\leq 20$  nm) were they  $> 1$  T [27]. Disordered superconducting systems are known to exhibit enhanced  $H_c$  [29,30]. Since  $S$  contacts the highly disordered NPF,  $S$  in turn may be disordered near the interface, leading to similarly enhanced  $H_c$  and broad ZFCs [13,31]. Conductance peaks as a function of  $V$ , too, are remarkably broad:  $\sim 2$  orders of magnitude greater than  $2\Delta/e$ , where  $\Delta$  is the energy gap of bulk  $S$ . Frydman and Dynes also observed RT features beyond  $2\Delta/e$  and attributed the broadening to voltage drops experienced by electrons in the  $N$  metal [6]. In the present system, the cause of ZBCP broadening is not known. We speculate that it is at least partially due to division of  $V$ ; i.e., interfering charges might encounter regions of high resistance near the NPF- $S$  interface, contributing to ZBCP broadening. Disorder in  $S$  might also account for some enhancement of  $\Delta$  at the DN- $S$  interface [30].

In summary, we find that molecularly-linked Au NPF- $S$  systems routinely exhibit robust QEMCO (via both  $V$ - and  $B$ -dependent measurements) predicted by a RT model. Oscillations persist to  $|B| \gg H_c$  of the bulk  $S$  in associa-

tion with nanostructured nature of the interface. Our results highlight the usefulness of NPFs for studying charge transport, particularly quantum interference and superconducting phenomena.

The authors thank A. Zabet-Khosousi for producing Au nanoparticle solutions; and J. Wei, Y.-J. Kim, and H. Zhang for access to the PPMS. This work was supported by the Natural Science and Engineering Research Council of Canada and the Institute of Optical Sciences, U. of Toronto.

\*adhirani@chem.utoronto.ca

- [1] A. Kastalsky *et al.*, Phys. Rev. Lett. **67**, 3026 (1991).
- [2] P. H. C. Magnée *et al.*, Phys. Rev. B **50**, 4594 (1994).
- [3] B. J. van Wees *et al.*, Phys. Rev. Lett. **69**, 510 (1992).
- [4] C. W. J. Beenakker, Phys. Rev. B **46**, 12 841 (1992).
- [5] I. K. Marmorosk, C. W. J. Beenakker, and R. A. Jalabert, Phys. Rev. B **48**, 2811 (1993).
- [6] A. Frydman and R. C. Dynes, Phys. Rev. B **59**, 8432 (1999).
- [7] J. M. Rowell and L. Y. L. Shen, Phys. Rev. Lett. **17**, 15 (1966).
- [8] B. L. Altshuler, A. G. Aronov, and P. A. Lee, Phys. Rev. Lett. **44**, 1288 (1980).
- [9] M. E. Gershenson, V. N. Gubankov, and M. I. Faley, Zh. Eksp. Teor. Fiz. **90**, 2196 (1986) [Sov. Phys. JETP **63**, 1287 (1986)].
- [10] A. M. Rudin, I. L. Aleiner, and L. I. Glazman, Phys. Rev. B **55**, 9322 (1997).
- [11] G. Deutscher, Rev. Mod. Phys. **77**, 109 (2005).
- [12] Z. D. Kvon *et al.*, Phys. Rev. B **61**, 11 340 (2000).
- [13] A. M. Marsh, D. A. Williams, and H. Ahmed, Semicond. Sci. Technol. **10**, 1694 (1995).
- [14] J. Nitta, T. Akazaki, and H. Takayanagi, Phys. Rev. B **49**, 3659 (1994).
- [15] I. Žutić and O. T. Valls, Phys. Rev. B **60**, 6320 (1999).
- [16] I. Žutić and O. T. Valls, Phys. Rev. B **61**, 1555 (2000).
- [17] T. M. Klapwijk, J. Supercond. **17**, 593 (2004).
- [18] H. Takayanagi, E. Toyoda, and T. Akazaki, Physica (Amsterdam) **367C**, 204 (2002).
- [19] N. Kim *et al.*, Solid State Commun. **115**, 29 (2000).
- [20] P.-E. Trudeau *et al.*, J. Chem. Phys. **117**, 3978 (2002).
- [21] A. Zabet-Khosousi *et al.*, Phys. Rev. Lett. **96**, 156403 (2006).
- [22] M. Brust *et al.*, Adv. Mater. **7**, 795 (1995).
- [23] M. Brust and C. J. Kiely, Colloids Surf. A **202**, 175 (2002).
- [24] J. B. Peška *et al.*, Appl. Phys. Lett. **89**, 063110 (2006).
- [25] J. L. Dunford, A.-A. Dhirani, and B. W. Statt, Phys. Rev. B **74**, 115417 (2006).
- [26] J. L. Dunford *et al.*, Phys. Rev. B **72**, 075441 (2005).
- [27] J. L. Dunford and A.-A. Dhirani, Nanotechnology **19**, 025202 (2008).
- [28] G. E. Blonder, M. Tinkham, and T. M. Klapwijk, Phys. Rev. B **25**, 4515 (1982).
- [29] F.-Y. Wu *et al.* J. Appl. Phys. **101**, 09G111 (2007).
- [30] G. A. Gibson, P. M. Tedrow, and R. Meservey, Phys. Rev. B **40**, 137 (1989).
- [31] A. M. Marsh, D. A. Williams, and H. Ahmed, Physica (Amsterdam) **203B**, 307 (1994).